Journal of Membrane Science and Research 6 (2020) 416-423

Journal of Membrane Science & Research

journal homepage: www.msrjournal.com

Research Paper

Novel Nanocomposite HNT-TiO_2/PVDF Adsorptive Nanofiber Membranes for Arsenic (III) Removal

Ali Moslehyani [1], Ramin Farnood [1,*], Shahram Tabe [1,2], Takeshi Matsuura [3], Ahmad Fauzi Ismail [4]

[1] *Department of Chemical Engineering and Applied Chemistry, University of Toronto, Toronto, Ontario M5S 3E5, Canada*
[2] *Ministry of the Environment, Conservation and Parks, Toronto, ON, M4V 1M2, Canada*
[3] *Department of Chemical and Biological Engineering, University of Ottawa, 161 Louis Pasteur St., Ottawa, ON K1N 6N5, Canada*
[4] *Advanced Membrane Technology Research Centre (AMTEC), Faculty of Chemical and Energy Engineering, Universiti Teknologi Malaysia, 81310 Skudai, Malaysia*

Article info

Received 2020-08-19
Revised 2020-09-24
Accepted 2020-09-25
Available online 2020-09-25

Keywords

Nanofiber
Adsorption
PVDF
HNT
TiO_2
As(III)

Highlights

- TiO_2-HNTs nanoparticles were successfully embedded in the ENAMs.
- Incorporating TiO_2-HNTs in ENAM increased the hydrophobicity of nanofibers.
- TiO_2-HNTs addition improved the As(III) adsorption capacity of ENAMs.
- EANMs performed well after cleaning with H_2O/NaOH solution and flushing with water.

Graphical abstract

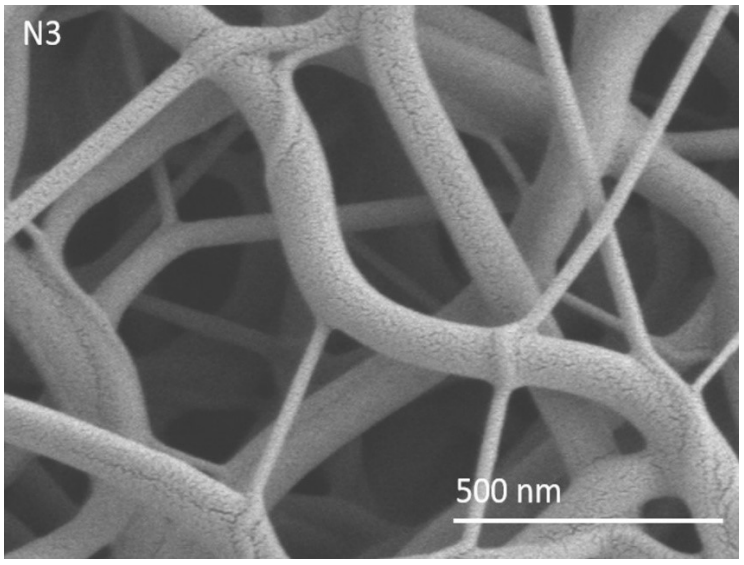

Abstract

In this work, the removal of arsenic (III) from contaminated water by means of electrospun nanofiber adsorptive membranes (ENAMs) has been reported. Polyvinylidene fluoride (PVDF) was used for preparation of the ENAMs incorporating titanium dioxide (TiO_2)-halloysite nanotubes (HNTs) nanoparticles as adsorbents. Removal of arsenic (III) by the prepared ENAMs was studied at adsorbent to polymer ratios of 0, 0.25, and 0.5 w/w. The addition of TiO_2-HNTs to the polymer left visible changes on the structural morphology and fibers properties of the membrane. The membrane samples were characterized by pure water permeability, contact angle measurement, TEM, SEM, XPS, and XRD. Results indicated that by increasing the TiO_2-HNT content, the adsorption capacity of the membrane improved. A maximum of 31.2 mg/g of arsenic adsorption was achieved using TiO_2-HNT to PVDF ratio of 0.5 w/w. The ENAMs were able to reduce the arsenic (III) concentration to less than 10 ppb, the level recommended by the World Health Organization (WHO). Moreover, the adsorptive properties of the nanocomposite fibers were restored to 94% of the original capacity by cleaning the membranes using sodium hydroxide solution followed by DI water flushing.

1. Introduction

Arsenic is found in earth's crust in more than 200 different minerals. Leaching of this naturally occurring arsenic has resulted in the persistent contamination of groundwater supplies in several countries around the world including Bangladesh, India and Taiwan [1,2]. This has created a significant human health challenge as arsenic is known to cause bladder, lungs, skin, and kidney cancers [3-6]. Accordingly, the World Health Organization (WHO) has set the a maximum limit of 10 ppb for arsenic in drinking water [7,8].

Various methods have been experienced for arsenic removal including

* Corresponding author: ramin.farnood@utoronto.ca (R. Farnood)

DOI: 10.22079/JMSR.2020.135081.1407

chemical and electrochemical treatment, ion exchange, adsorption, and membrane filtration [9-14]. An emerging technology that offers promise in removing arsenic is membrane adsorption (MA). MA combines adsorption and membrane filtration technologies as an efficient method for treating contaminated waters [15-18]. Considering various MA techniques, electrospun nanofiber adsorptive membranes (ENAMs) are of particular interest due to their high permeation rate and adsorption capacity [18-23].

ENAMs are often functionalized via nanoparticles addition to enhance their performance and adsorption capacity. One of such nanomaterials is halloysite nanotube or HNT ($Al_2Si_2O_5(OH)_4$). HNT is typically 0.5 to 10 nm long, has an inner diameter of 12-15 nm and an outer diameter of 50-60 nm. The outer surface of HNT is mostly composed of SiO_2 and its inner surface is composed of Al_2O_3, hence, it serves as an excellent support material for metal oxides [24-28]. Earlier studies have shown that immobilization of titanium dioxide nanoparticles on HNT improved TiO_2 dispersion and prevented its aggregation [27,29]. Compared to carbon nanotubes, HNTs disperse better in water, are reused more readily, and are cheaper [30,31]. Therefore, immobilization of TiO_2 on the HNT surface offers a promising approach for the removal of arsenic via adsorption [26].

In this study, we reported the preparation and characterization of electrospun nanofibre membranes containing HNT-TiO_2 nanoparticles for the removal of As(III) from contaminated water.

2. Methodology

2.1. Materials

Polyvinylidene fluoride (PVDF® 761) was purchased in pellet form from Kynar polymer. Dimethylacetamide (DMAc, >99.5%), polyvinylpyrrolidone (PVP), halloysite nanotubes (5~15 nm inside diameter), N-β-(aminoethyl)-γ-aminopropyltrimethoxy silane (AEAPTMS), sodium arsenite ($NaAsO_2$), toluene, tetra hydro furane (THF) and acetone (>99.3%) were purchased from Sigma Aldrich. Titanium dioxide P25 (surface area 50±15 m^2/g) were purchased from Degussa and Merck supplied sodium hypochlorite (NaClO) and NaOH.

2.2. HNT-TiO_2 synthesis

To immobilize TiO_2 on HNTs surface, 10 g of AEAPTMS was dissolved in 100 mL of toluene via sonication. 10 g TiO_2 and 10 g HNTs were then introduced and the suspension was heated under reflux at 95 ºC for 24 h. TiO_2-HNT was rinsed first with 500 mL THF and then with 500 mL distilled water to remove free TiO_2 and HNTs. TiO_2-HNT produced in this way was separated and dried at 85 ºC for 48 h.

2.3 Dope preparation and spinning procedure

ENAM polymer dope was prepared by dissolving a pre-weighed amount of PVP as pore forming agent and HNTs-TiO_2 in DMAc and sonicated for almost 4 h, followed by mechanical stirring for 12 h to minimize HNTs-TiO_2 agglomeration. PVDF polymer and acetone as non-solvent were then added to the dope, which was also sonicated for an hour to remove air bubbles. The composition of the electro-spinning dope is given in Table 1. The spinning dope was extruded from a 30 mL plastic syringes via a 27-gauge stainless needle (outer diameter 0.4 mm, length 10 mm) at 32 ºC. The voltage was 15 kV, the extrusion flow rate was 1.6 mL/h, and the needle was kept at a fixed distance of 15 cm from the collector. The electrospinning process was conducted at 32 ºC. The collector was wrapped with aluminum foil covered by polyethylene terephthalate (PET) nonwoven support. The ENAMs were pill off collected after 10 h of electrospinning.

Table 1
Polymer dope composition for ENAM preparation. The ratio of DMAc to acetone was 9.5:0.5.

ENAM	PVDF:HNT-TiO_2	(w/w) %			
		HNT-TiO_2	PVDF	PVP	DMAc+Acetone
N1	1:0	0.0	15.0	2.0	83.0
N2	1:0.25	3.7	14.4	1.9	80.0
N3	1:0.50	6.9	13.9	1.8	77.4

2.4. Characterization of nanoparticles and ENAMs

Transmission electron microscope (TEM) Hitachi (HT 7700) was used to observe TiO_2-HNTs after the nanoparticles were dispersed in either methanol or ethanol under sonication for 10 min. To examine the structure of ENAMs, a Hitachi (SU 5000 VP) field emission scanning electron microscope (FESEM) was employed. Samples were mounted on FESEM stubs a carbon tape prior being gold coated (carbon paint used on one corner of samples to ensure good conductivity).

A K-Alpha X-ray photoelectron spectroscopy (XPS) system from Thermo Fisher Scientific (East Grinstead, UK) was used to examine the ENAMs chemical composition. The system used a micro-focused X-ray using a 400µm spot with charge compensation, while a low energy flood of electrons and ions was used as required. Under these conditions, the vacuum pressure within the analytical chamber was about 5×10^{-8} mbar. Without charge compensation, the analysis chamber vacuum was in the 10^{-9} mbar range. Moreover, X-ray diffraction analysis (XRD) was confirming compatibility of TiO_2-HNTs and PVDF in ENAMs. The video-based optical contact angle measuring system was purchased from Data Physics Instruments (OCA 15EC). The surface hydrophilicity was obtained by membrane placing on the contact angle machine and dropping a 5 µL deionized drop of water to the membrane surface and then capturing by digital camera located inside the contact angle machine which was connected to a computer.

2.5. Adsorption experiment

0.2 g of ENAM sample was added to 200 mL of an aqueous solution of $NaAsO_2$. The sample was mixed continuously at 400 rpm for 24 h at room temperature using a shaker. Arsenic concentration was determined using an inductive coupled plasma - mass spectrometry (ICP-MS) and inductively coupled plasma - optical emission spectrometry (ICP-OES) analysis provided by Thermo Scientific. The ENAM adsorption capacity was examined in the pH range 2 to 11 using 10 ppm aqueous As(III) solution. The pH was adjusted by adding NaOH solution. In this experiment arsenic ion reduction percentage was defined as %R:

$$\%R = \left(\frac{C_e}{C_i}\right)\times 100 \quad (1)$$

where C_i and C_e (in ppm) represent arsenic concentrations at the start of the adsorption experiments and after 24 h, respectively. The adsorption isotherm was established by using aqueous solutions of different arsenic concentrations (100, 150, 200, and 250 ppb). The equilibrium amount of arsenic adsorbed on to ENAMs, q_e(µg.g^{-1}), was determined from:

$$q_e = \frac{V}{M_m}\times(C_i - C_e) \quad (2)$$

where V is the solution volume and M_m is the mass of ENAM sample.

Adsorption kinetics study was carried out under the same conditions as the adsorption isotherm study, except for the initial arsenic concentration, C_i, of 40 ppm. The amount of adsorbed arsenic at a given time, q_t (mg. g^{-1}), was calculated following a similar approach and using the measured arsenic concentration at time t, i.e. C_t.

2.6. Dynamic adsorption experiment

For filtration experiments, a crossflow ultrafiltration set-up equipped with a permeation cell (effective area 12.56 cm^2) was used, as seen in Figure 1. To minimize compaction effects during the pure water permeation test, ENAM was first pressurized to 2 bar and was maintained at this pressure for 30 min. The pressure was subsequently reduced to 0.1 bar and permeate was collected over a period of 30 min. The pure water flux was then calculated from:

$$J = \frac{V}{A\times t} \quad (3)$$

where V is the cumulative volume of permeate obtained during time t and A is the surface area of the membrane. To test the removal of As(III), the feed solution containing 103.8 ppb As(III) was pumped from a feed tank to the permeation cell and recycled to the feed tank. Solution volume in the feed tank was maintained at 5.5 L by adding make-up solution from time to time. Filtration experiments for a feed solution was operated for only N3 with low As(III) concentration of pH at 6.7 and pressure equal to 1.0 barg.

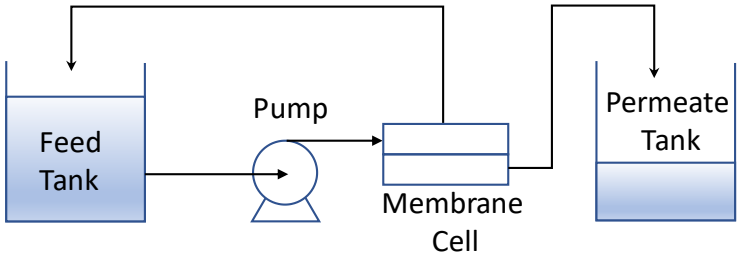

Fig. 1. A general scheme of the nanocomposite dynamic adsorption set-up.

3. Result and discussions

3.1. Characterization of adsorbent and ENAMs

TEM characterization was applied for the raw HNTs and modified HNTs-TiO_2 to reveal the immobilization of TiO_2 on the surface of HNTs. TEM micrographs confirm that TiO_2 nanoparticles were deposited on the surface of the HNTs (Figure 2).

Figure 3 shows the X-ray diffraction (XRD) characteristics for (a) immobilized HNTs-TiO_2 adsorbent, (b) PVDF membrane without HNTs+TiO_2 (N1) and (c) PVDF membrane with HNTs+TiO_2 (N3). The XRD patterns of immobilized HNTs-TiO_2 adsorbent showed the 3 crystalline spectra at 2θ of 12.9, 22.5, 27.4.1, 42.1, 53.7, 61.5 and 71.0. The N3 also possessed similar crystalline patterns at 2 θ of 13.4, 22.9, 28.2, 42.8, 54.3, 62.1 and 71.8. The XRD spectra confirm the presence of HNTs-TiO_2 nanoparticles and showed that HNT-TiO_2 addition resulted in changing PVDF crystal structure from α-crystalline phase in N1 to β-crystalline phase in N3.

Figure 4 shows FESEM images of the three nanofiber membranes (N1, N2 and N3). As shown, the surfaces of ENAMs N2 and N3 membranes are different from the pristine PVDF nanofiber (N1). The average fiber diameters are below 150 nm for all nanofiber membranes. Also, formation of spider web fibers (thinner than an extended from the trunk fibers) is of importance.

XPS analysis was used to determine the elemental composition of the membranes as listed in Table 2. The results confirm the enhancement of TiO_2 in N3 membrane compared to N2. The increase is expected to enhance the adsorption capacity of N3 compared with N1 and N2, as will be discussed later.

Table 2
Elemental analysis of ENAMs using XPS (in at %).

ENAM	C	F	Ti	Others
N1	60	39	0	1
N2	53	37	8	2
N3	52	35	9	4

The contact angle, overall porosity, pure water permeation flux (at 0.1 bar_g), and theoretical specific surface area, *S*, of the fiber estimated based on Eq. 4 are listed in Table 3:

$$S = \frac{2\pi r l}{M_m} \quad (4)$$

Where *r* is the average nanofibers radius, *l* is the total fibers length, and M_m is the mass of the ENAM sample.

The results indicate that addition of HNTs-TiO_2 substantially decreases contact angle of the membranes and turn them from hydrophobic to hydrophilic. This is also reflected in the significant enhancement in pure water flux in N2 and N3 compared to N1. The average fiber diameter also decreases with the addition of HNTs-TiO_2, which is probably due to conductivity enhancement of the polymer solution and the ejected filament.

Table 3
Properties of electrospun nanofiber adsorption membrane samples.

ENAM	Contact angle (º)	Pure water flux (L. m^{-2}. h^{-1})	Theoretical specific surface area ($m^2.g^{-1}$)
N1	100	973	16.8
N2	45	4176	17.3
N3	20	5035	17.9

* Effective area of ENAM was 12.6 cm^2.

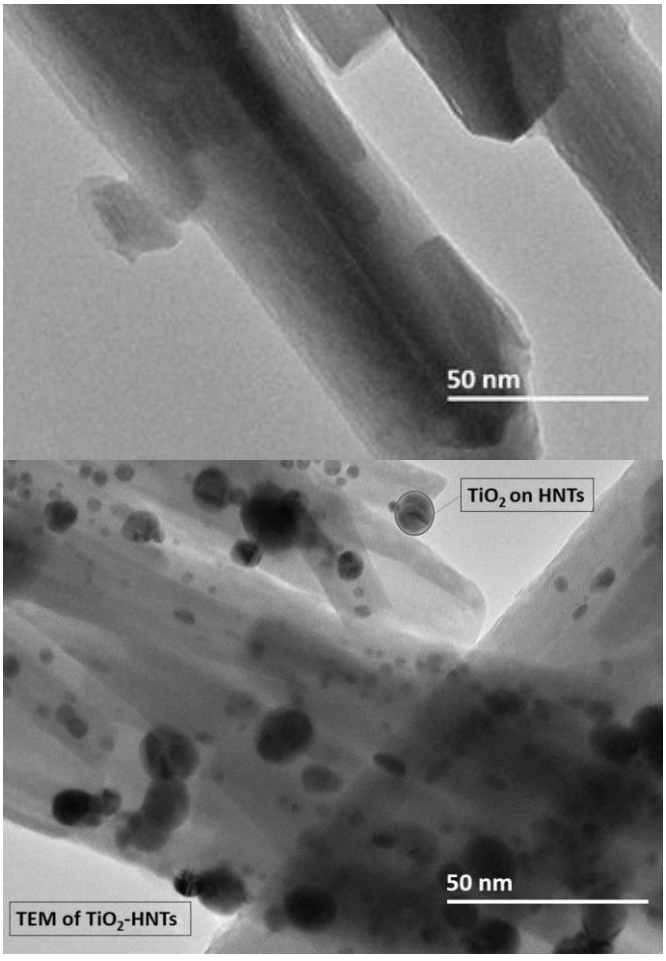

Fig. 2. TEM images of TiO_2-HNTs adsorbent.

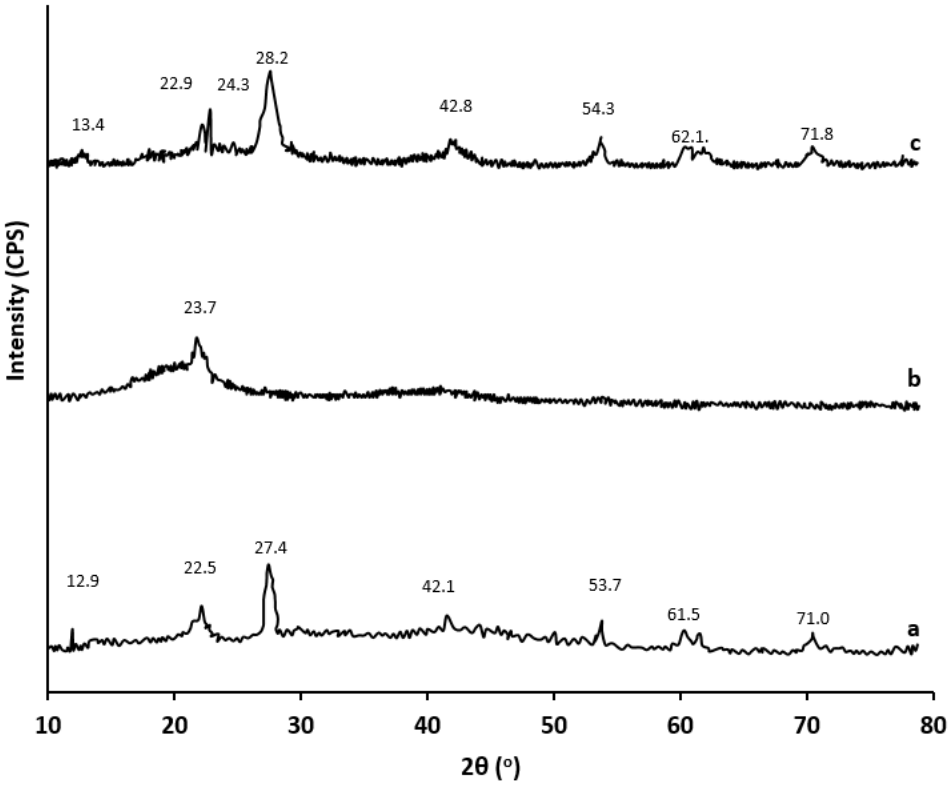

Fig. 3. XRD spectra of (a) HNTs-TiO_2 adsorbent, (b) N1 and (c) N3.

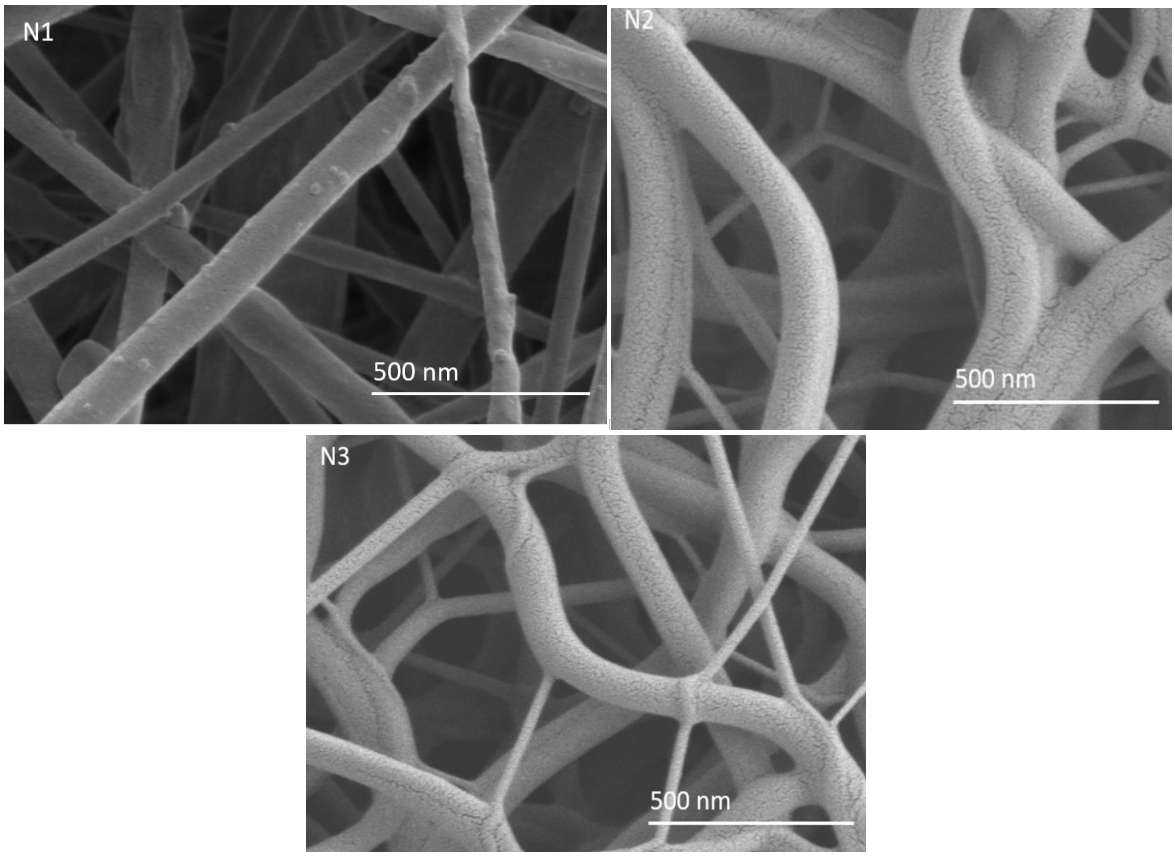

Fig. 4 FESEM images of N1, N2, and N3. Scale bar is 500 nm.

3.2. Adsorption analysis

3.2.1. Effect of pH

The dependency of As(III) adsorption on water pH was examined through a series of experiments using N3 membrane. For this purpose, the adsorption of As(III) was determined at pH values between 2 and 11. The results are shown in Figure 5, which indicate that removal of As(III) was maximum in more acidic region. The adsorption started to decline at higher pH values. That is because arsenate ion has a negative charge enhancing arsenic adsorption by electrostatic attraction. The degree of protonation decreases with increasing pH leading to a decline in arsenic ion adsorption.

3.2.2. Adsorption isotherm

Figure 6 depicts adsorption isotherms for N1, N2, and N3 membranes at pH equal to 3. This pH was selected because – as it was shown in previous Section – the arsenic adsorption was maximum. As expected, the membrane with no HNTs-TiO_2 (N1) showed the lowest adsorption capacity. A jump in the capacity was observed when HNTs-TiO_2 was added to membranes N2 and N3. However, no linear relationship was observed between amount adsorbed and TiO_2 loading. That is, while the TiO_2 content of N3 membrane was twice as high as that in N2, the adsorption capacity enhanced only a few percentage points. The highest adsorption capacity was 185.6 $\mu g.g^{-1}$ for N3 when As(III) concentration in the feed was 250 ppb. The adsorption capacities are expected to slightly lower at pH = 6 to 8. Comparison with data provided in Table 3 shows that the increase in the Langmuir adsorption capacity was proportional to the theoretical specific surface area of the membrane (R^2 = 0.90). This suggests that increase in the adsorption capacity by HNTs-TiO_2 addition was likely caused by the increase in the specific surface area of the membrane.

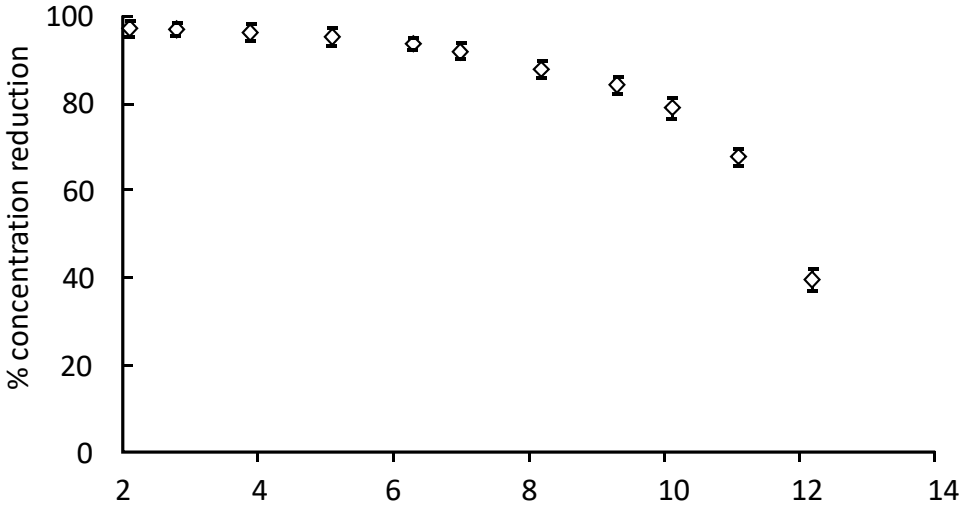

Fig. 5. The effect of pH on arsenic removal by N3.

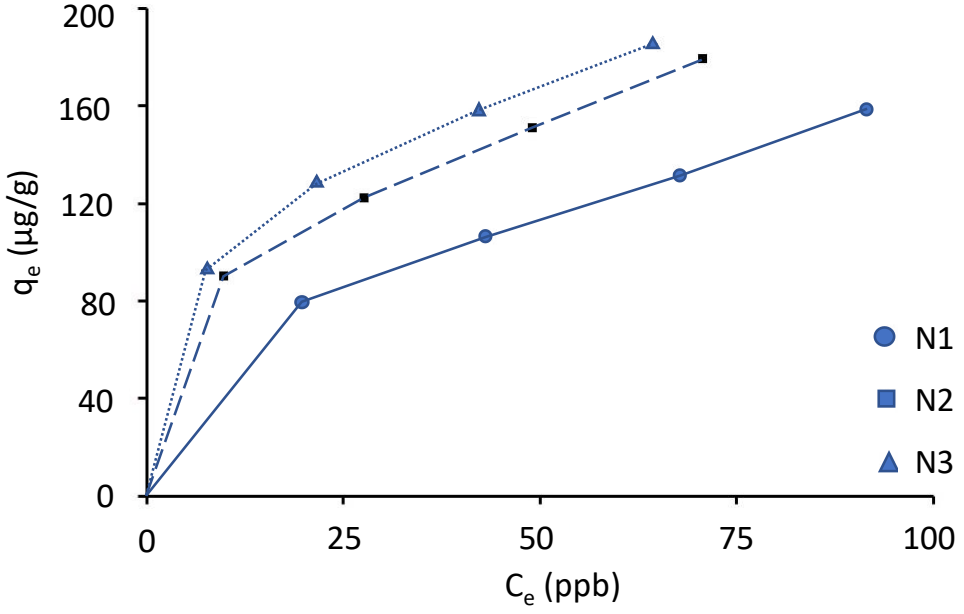

Fig. 6. Isotherm experimental data for N1, N2, and N3.

Langmuir and Freundlich isotherms, given by Equations (5) and (6), were used to fit the adsorption data:

$$q_e = \frac{mbC_e}{1+bC_e} \quad (5)$$

$$q_e = K_f C_e^{1/n} \quad (6)$$

where m is the monolayer adsorption capacity (mg.g^{-1}), b is the Langmuir constant (L.mg^{-1}), $1/n$ is the heterogeneity factor, and K_f represents the Freundlich constant (µg.g^{-1}).

The results of the regression analyses are given in Table 4. According to Table 4, the experimental results exhibited a better fit with the Langmuir model as evident by the correlation coefficients (R^2), suggesting that monolayer adsorption was likely a more dominant mechanism in arsenic removal by ENAMs.

3.2.3. Adsorption kinetics

Figure 7 shows the variation of As(III) amount adsorbed versus time using N3 ENAM at initial feed concentration of 40 ppm. The adsorption kinetic was obtained using Lagergren's pseudo-first and second order kinetics given by Equations (7) and (8), respectively.

$$q_t = q_e(1-\exp(-K_1 t)) \quad (7)$$

$$q_t = \frac{q_e^2 K_2 t}{1+q_e K_2 t} \quad (8)$$

here, q_e and q_t (both in mg.g^{-1}) are the equilibrium and instantaneous amount of arsenic, respectively, adsorbed onto ENAMs, K_1 (h^{-1}) is the pseudo first order rate constant, and K_2 (g.mg^{-1}.h^{-1}) is the pseudo second order rate constant. The estimated values for model parameters are listed in Table 5. While the correlation coefficients (R^2) were above 0.9 for both kinetic models, a comparison between the actual and theoretical results indicated better fit with the second order kinetics.

3.3. Permeation experiments

As shown in Figure 8, arsenic concentration increased in permeate progressively and reached to 10 ppb, which is considered the maximum safe level based on the WHO, after the permeate volume of 1.3 L. Concentration of arsenic in permeate further increased to 18 ppb after 2.0 L of permeate was collected at which point the experiment was stopped and the membrane was regenerated using a mild caustic solution, followed by flushing with DI water. The regenerated membrane produced a similar performance, treating a total volume of 1.3 L of contaminated feed before reaching a permeate concentration of 10 ppb, as shown in Figure 8. The reproducibility was defined as the ratio of the permeate volume when the concentration reached 10 ppb in the second cycle to that in the first cycle. The reproducibility in this study was 93.7%. It should be noted that TiO_2 were leached to the permeate solution negligibly, which was less than 8 ppb during all of experiments. The breakthrough volume, defined as C_t/C_o = 0.05, for both fresh and regenerated membranes was 0.44 L. However, breakthrough volume is a strong function of the feed flow rate. Earlier studies have shown that permeate concentration increased exponentially with increasing flow rate, as adsorbate compounds could passed through the membrane due to insufficient contact time [32]. Therefore, it is expected that breakthrough volume will decrease as flow rate increases.

Table 4
Langmuir and Freundlich model parameters for arsenic adsorption by ENAMs.

ENAM	Langmuir model			Freundlich model		
	m (µg.g^{-1})	b (L.mg^{-1})	R^2	1/n (–)	K_f (µg.g^{-1})	R^2
N1	181	0.06	0.996	2.2	1.04×10^{-3}	0.988
N2	189	0.11	0.994	2.8	2.45×10^{-5}	0.961
N3	192	0.20	0.999	3.1	6.35×10^{-6}	0.947

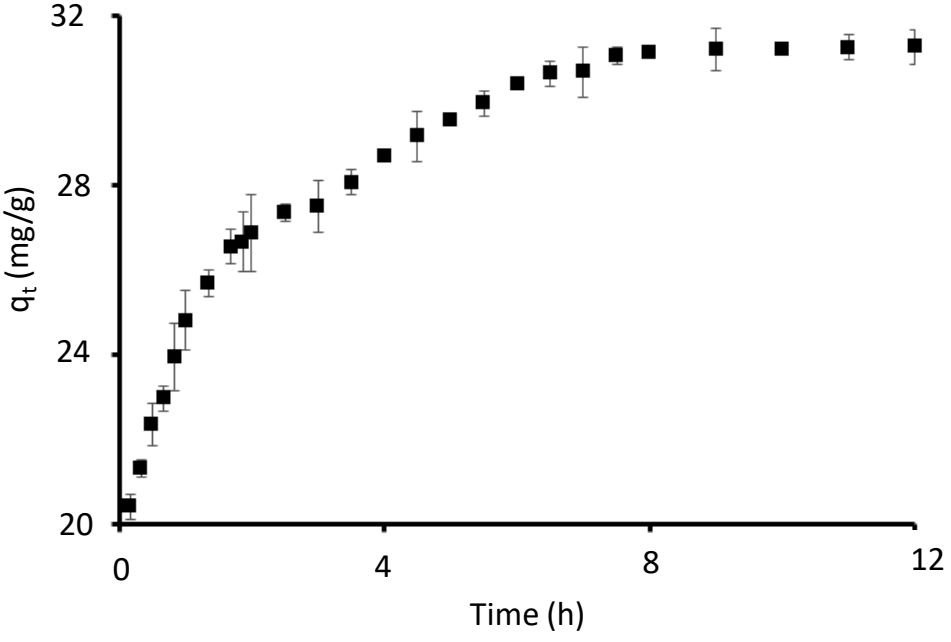

Fig. 7. Adsorbed amount versus time (membrane, N3; C_i = 40 ppm; ENAM = 0.2 g; solution volume = 0.2 L).

Table 5
Estimated parameters for first and second order adsorption kinetic models determined using linear regression.

C_i (ppm)	q_e (mg.g^{-1})	1st order			2nd order		
		q_{e1} (mg.g^{-1})	K_1 (h^{-1})	R^2	q_{e2} (mg.g^{-1})	K_2 (g.mg^{-1}.h^{-1})	R^2
40	31.2	20.2	0.592	0.964	31.9	0.106	0.999

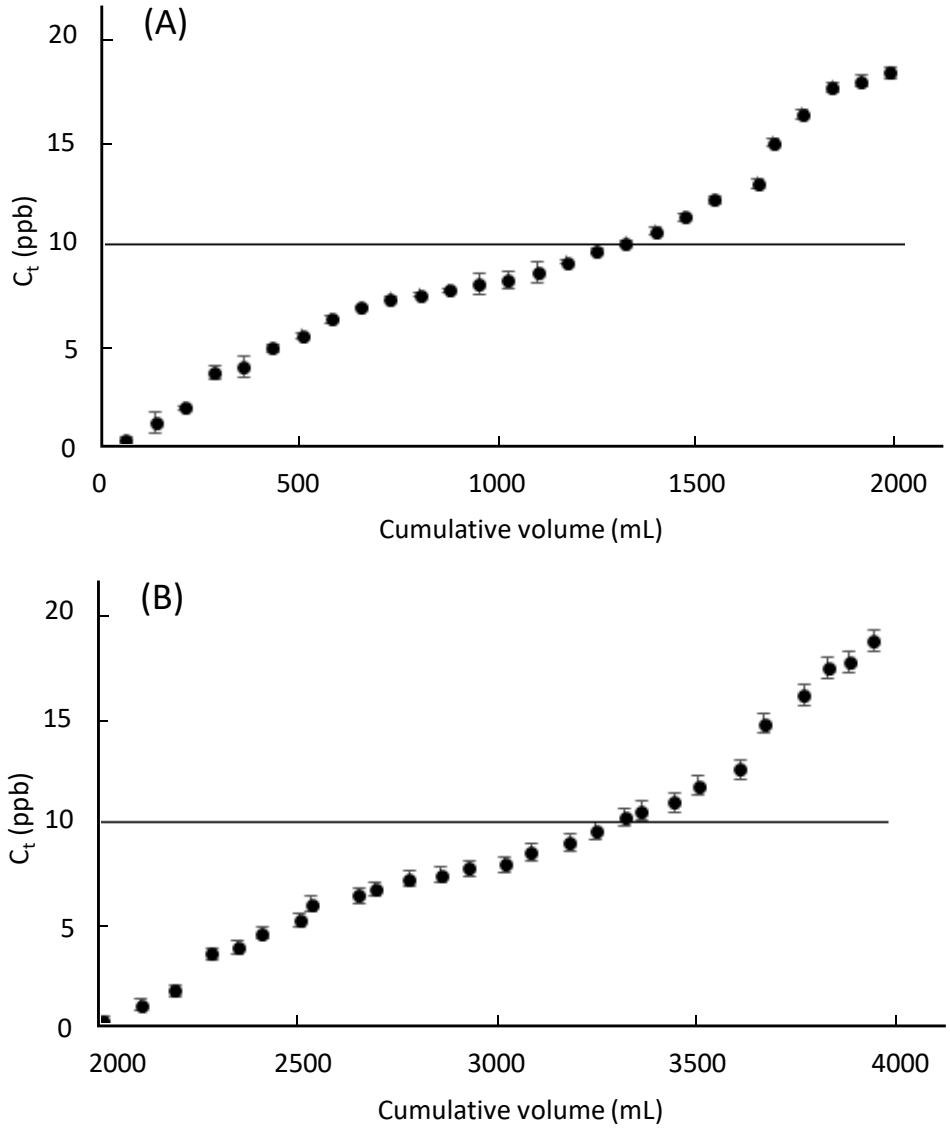

Fig. 8. Results of filtration experiment with low As(III) concentration in the feed (concentration = 103.8 ppb; operating pressure = 1 barg, pH = 3) (A) first cycle (B) After membrane cleaning.

4. Conclusions

The TiO_2-HNT/PVDF ENAMs were fabricated and tested for As(III) adsorption and filtration in this investigation. From the investigational results lead to the following conclusions:

1. The TiO_2-HNTs nanoparticles could be successfully synthesized.
2. TiO_2-HNTs nanoparticles could be embedded in the ENAMs,
3. Incorporated TiO_2-HNTs in ENAMs was significantly increased the hydrophobicity, overall porosity, length of the fibers, and specific surface of the fiber.
4. Furthermore, TiO_2-HNTs was improved the As(III) adsorption significantly.
5. Langmuir isotherm and pseudo second order kinetic model exhibited a better fit with the experimental data than the Feurndlich isotherm and pseudo-first order model.
6. Finally, large volumes of clean permeate could be collected by using the crossflow filtration set-up. Thus more, ENAMs also could be used after restoration by cleaning with NaOH solution following by flushing with DI water.

Acknowledgments

The authors gratefully acknowledge financial support by Natural Sciences and Engineering Research Council of Canada (NSERC) of Grant STPGP 463039-14 and University of Ottawa. Moreover, authors wish to thank the Ministry of Higher Education of Malaysia and University Technology Malaysia (UTM) for technical and financial support via Grant Vote R.J090301.7809.4J195.

References

[1] J.A. Baig, T.G. Kazi, M.B. Arain, H.I. Afridi, G.A. Kandhro, R.A. Sarfraz, M.K. Jamal, A.Q. Shah, Evaluation of arsenic and other physico-chemical parameters of surface and ground water of Jamshoro, Pakistan, J Hazard Mater, 166 (2009) 662-669. doi: 10.1016/j.jhazmat.2008.11.069

[2] M. Filella, N. Belzile, Y.-W. Chen, Antimony in the environment: a review focused on natural waters: I. Occurrence, Earth Sci Rev, 57 (2002) 125-176. doi: 10.1016/S0012-8252(01)00070-8

[3] A.H. Welch, D. Westjohn, D.R. Helsel, R.B. Wanty, Arsenic in ground water of the United States: occurrence and geochemistry, Ground water, 38 (2000) 589-604. doi: 10.1111/j.1745-6584.2000.tb00251.x

[4] T. G. Rossman, Molecular and Genetic Toxicology of Arsenic, in Environmental Toxicology: Current Developments. J. Rose (ed). Gordon and Breach Science Publishers, Amsterdam, 1998, pp.175-192.

[5] J. Buschmann, M. Berg, C. Stengel, L. Winkel, M.L. Sampson, P.T.K. Trang, P.H. Viet, Contamination of drinking water resources in the Mekong delta floodplains: Arsenic and other trace metals pose serious health risks to population, Environ Int, 34 (2008) 756-764. doi: 10.1016/j.envint.2007.12.025

[6] S. Wang, C.N. Mulligan, Occurrence of arsenic contamination in Canada: sources, behavior and distribution, Sci Total Environ, 366 (2006) 701-721. doi: 10.1016/j.scitotenv.2005.09.005

[7] R. Stone, Arsenic and paddy rice: a neglected cancer risk?, Science, 321 (2008) 184-185. doi: 10.1126/science.321.5886.184

[8] R.Y. Ning, Arsenic removal by reverse osmosis, Desalination, 143 (2002) 237-241. doi: 10.1016/S0011-9164(02)00262-X

[9] R.J. Gohari, W. Lau, T. Matsuura, A. Ismail, Fabrication and characterization of novel PES/Fe–Mn binary oxide UF mixed matrix membrane for adsorptive removal of As (III) from contaminated water solution, Sep Purif Technol, 118 (2013) 64-72. doi: 10.1016/j.seppur.2013.06.043

[10] D. Mohan, C.U. Pittman, Arsenic removal from water/wastewater using adsorbents—a critical review, J Hazard Mater, 142 (2007) 1-53. doi: 10.1016/j.jhazmat.2007.01.006

[11] M. Bissen, F.H. Frimmel, Arsenic—a review. Part II: oxidation of arsenic and its removal in water treatment, CLEAN–Soil, Air, Water, 31 (2003) 97-107. doi: 10.1002/aheh.200300485

[12] E.O. Kartinen, C.J. Martin, An overview of arsenic removal processes, Desalination, 103 (1995) 79-88. doi: 10.1016/0011-9164(95)00089-5

[13] M.F. Ahmed, An overview of arsenic removal technologies in Bangladesh and India, in: Proceedings of BUET-UNU international workshop on technologies for arsenic removal from drinking water, Dhaka, 2001, pp. 5-7.

[14] A.S. Chen, L. Wang, J.L. Oxenham, W.E. Condit, T.J. Sorg, W. Supply, Capital Costs of Arsenic Removal Technologies: US EPA Arsenic Removal Technology Demonstration Program Round 1, in, EPA/600/R-04/201. US Environmental Protection Agency, National Risk Management Research Laboratory, Cincinnati, OH, 2004.

[15] C. Chuang, M. Fan, M. Xu, R. Brown, S. Sung, B. Saha, C. Huang, Adsorption of arsenic (V) by activated carbon prepared from oat hulls, Chemosphere, 61 (2005) 478-483. doi: 10.1016/j.chemosphere.2005.03.012

[16] H. Genç-Fuhrman, J.C. Tjell, D. McConchie, Adsorption of arsenic from water using activated neutralized red mud, Environ Sci Technol, 38 (2004) 2428-2434. doi: 10.1021/es035207h

[17] R.J. Gohari, W.J. Lau, E. Halakoo, A.F. Ismail, F. Korminouri, T. Matsuura, M.S.J. Gohari, M.N.K. Chowdhury, Arsenate removal from contaminated water by a highly adsorptive nanocomposite ultrafiltration membrane, New J Chem, 39 (2015) 8263-8272. doi:10.1039/c5nj00690b

[18] A. Moslehyani, T. Matsuura, A.F. Ismail, M.H.D. Othman, A review on application of electrospun polymeric nanofibers, in: National Congress on Membrane Technology 2016 (NATCOM 2016), Pulai Springs Resort, Johor Bahru, 24-25 August 2016.

[19] R. Sharma, N. Singh, A. Gupta, S. Tiwari, S.K. Tiwari, S.R. Dhakate, Electrospun chitosan–polyvinyl alcohol composite nanofibers loaded with cerium for efficient removal of arsenic from contaminated water, J Mater Chem A, 2 (2014) 16669-16677. doi: 10.1039/c4ta02363c

[20] D. Chauhan, J. Dwivedi, N. Sankararamakrishnan, Novel chitosan/PVA/zerovalent iron biopolymeric nanofibers with enhanced arsenic removal applications, Environ Sci Pollut R, 21 (2014) 9430-9442. doi: 10.1007/s11356-014-2864-1

[21] L.-L. Min, Z.-H. Yuan, L.-B. Zhong, Q. Liu, R.-X. Wu, Y.-M. Zheng, Preparation of chitosan based electrospun nanofiber membrane and its adsorptive removal of arsenate from aqueous solution, Chem Eng J, 267 (2015) 132-141. doi: 10.1016/j.cej.2014.12.024

[22] A.-m. Cao, J.D. Monnell, C. Matranga, J.-m. Wu, L.-l. Cao, D. Gao, Hierarchical nanostructured copper oxide and its application in arsenic removal, J Phys Chem C, 111 (2007) 18624-18628. doi: 10.1021/jp0773379

[23] A. Moslehyani, T. Matsuura, A.F. Ismail, M.H.D. Othman, Preparation and characterization of electro-spun nanofiber membranes (ENMs) for membrane adsorption, in: National Congress on Membrane Technology 2016 (NATCOM 2016), 2016.

[24] X. Gao, P.W. Huo, X.L. Liu, D. Wu, Z.Y. Lu, Y.S. Yan, Preparation of Nd3+/TiO2/HNTs by Ion Imprinting Technology and its Photodegradation Property on Tetracycline, Appl Mech Mater, 316 (2013) 1041-1044. doi: 10.4028/www.scientific.net/AMM.316-317.1041

[25] A. Moslehyani, A. Ismail, M. Othman, A.M. Isloor, Novel hybrid photocatalytic reactor-UF nanocomposite membrane system for bilge water degradation and separation, RSC Adv, 5 (2015) 45331-45340. doi: 10.1039/C5RA01491C

[26] A. Moslehyani, M. Mobaraki, T. Matsuura, A. Ismail, M. Othman, M. Chowdhury, Novel green hybrid processes for oily water photooxidation and purification from merchant ship, Desalination, 391 (2016) 98-104. doi: 10.1016/j.desal.2016.01.003

[27] R.S. Murali, M. Padaki, T. Matsuura, M. Abdullah, A. Ismail, Polyaniline in situ modified halloysite nanotubes incorporated asymmetric mixed matrix membrane for gas separation, Sep Purif Technol, 132 (2014) 187-194. doi: 10.1016/j.seppur.2014.05.020

[28] Y. Chen, Y. Zhang, J. Liu, H. Zhang, K. Wang, Preparation and antibacterial property of polyethersulfone ultrafiltration hybrid membrane containing halloysite nanotubes loaded with copper ions, Chem Eng J, 210 (2012) 298-308. doi: 10.1016/j.cej.2012.08.100

[29] A. Moslehyani, M. Mobaraki, A. Isloor, A. Ismail, M. Othman, Photoreactor-ultrafiltration hybrid system for oily bilge water photooxidation and separation from oil tanker, React Funct Polym, 101 (2016) 28-38. doi: 10.1016/j.reactfunctpolym.2016.02.003

[30] R. Wang, G. Jiang, Y. Ding, Y. Wang, X. Sun, X. Wang, W. Chen, Photocatalytic activity of heterostructures based on TiO_2 and halloysite nanotubes, ACS Appl Mater Inter, 3 (2011) 4154-4158. doi: 10.1021/am201020q

[31] L.-Y. Yu, H.-M. Shen, Z.-L. Xu, PVDF-TiO_2 composite hollow fiber ultrafiltration membranes prepared by TiO_2 sol-gel method and blending method, J Appl Polym Sci, 113 (2009) 1763-1772. doi: 10.1002/app.29886

[32] M. J. Soberman, R. R. Farnood, S. Tabe, Functionalized powdered activated carbon electrospun nanofiber membranes for adsorption of micropollutants. Sep Purif Technol 253 (2020) 117461. doi: 10.1016/j.seppur.2020.117461